DOI: 10.17725/rensit.2022.14.309

Light Diffraction by Flat Geometric Bifractals

Galina V. Arzamastseva, Mikhail G. Evtikhov, Fedor V. Lisovsky, Ekaterina G. Mansvetova

Kotelnikov Institute of Radioengineering and Electronics of RAS, Fryazinsky Branch, http://fire.relarn.ru/
Fryazino 141190, Moscow Region, Russian Federation

E-mail: arzamastseva@mail.ru, emg20022002@mail.ru, lisf@df.ru, mansvetova_eg@mail.ru

Received May 26, 2022, peer-reviewed June 6, 2022, accepted June 13, 2022

Abstract: **In the Fraunhofer zone, an experimental study of the diffraction of a collimated beam of light with a wavelength of 0.63 microns after passage through computer-generated images of flat geometric bifractals, which are a combination of two geometric fractals of different dimensions, was performed. The studies used bifractals based on the classical Vicsek fractal and two less well-known fractals of L-systems. The selected images were transferred to a transparent film using a phototypesetter with a resolution of 1333 dots per centimeter (3386 dpi) and a point size of 7.5 microns. Diffraction patterns were visually observed on the screen and recorded using a digital camera and then transmitted to a computer for processing. The diffraction patterns observed in optical experiments were compared with "digital" diffractograms, that is, with Fourier images of bifractal images approximated by a grid function on a uniform square grid at different values of the parameter used in calculations that determines the ratio between the overall size of the smallest element of the prefractal and the grid period.**

Keywords: **bifractal, diffraction, Fraunhofer zone, monofractal, prefractal, grid function, Vicsek fractal, L-system fractal, Fourier image**

UDC 51.74; 535.4

Acknowledgments: The work was carried out within the framework of the state task.

For citation: Galina V. Arzamastseva, Mikhail G. Evtikhov, Fedor V. Lisovsky, Ekaterina G. Mansvetova. Light diffraction by flat geometric bifractals. *RENSIT: Radioelectronics. Nanosystems. Information Technologies*, 2022, 14(3):309-316. DOI: 10.17725/rensit.2022.14.309.

Contents

1. INTRODUCTION

Previously, we proposed a method for constructing geometric bifractals based on the use of the "fractal-carrier – carryable prefractal" algorithm [1]. A number of bifractals were constructed, which are a pairwise combination of four geometric monofractals (the Serpinsky carpet or the Vicsek fractal and two L-system monofractals with an axiom in the form of a square), their digital megapixel pictures were obtained, and their digital Fourier images were calculated, the comparison of which with the corresponding diffraction patterns observed in the Fraunhofer region, in [1], however, was not performed due to the lack of experimental data. In this paper, which was carried out in order to eliminate this gap, the results of an experimental study of light diffraction for two of the bifractals mentioned in [1] are presented, in the first of which the carrier is

the Vicsek fractal, and the carryable is the LS1 fractal of the L-system (hereinafter referred to as bifractal No. 1), and in the second the carrier is the fractal L-system LS2, and the carryable is the LS1 fractal (hereinafter referred to as bifractal No. 2). General information and description of the fractals mentioned above can be found, for example, in [2-5].

To obtain Fourier spectra, we used the computer modeling method previously described by us in [6], which was first applied to real thermodynamically stable fractal-like domain structures [7] and was finally worked out on test objects, as which ordered domain structures realized in thin magnetic films were selected, allowing diffraction "to the lumen" [8]. The method was also applied in the study of abstract fractal objects: Koch's snowflake, Serpinsky carpet, Vicsek fractal, and others [9-13].

2. METHODS OF CONDUCTING EXPERIMENTS

For experimental research of diffraction by fractals, black-and-white bitmap pictures of selected objects were created on a computer using specially developed programs. The resulting pictures were printed by imagesetter on a transparent film with a resolution of 1333 dots per centimeter (3386 dpi) and a point size of 7.5 microns. The smallest fractal element was formed from 4-10 points, that is, its linear size ranged from 30 to 75 microns. The images obtained by the described method had an extremely high contrast, almost unattainable for traditional photography.

A standard technique was used to observe the diffraction pattern formed after the passage of a light beam through a transparent film with an picture of the prefractal diffraction pattern in the Fraunhofer zone. A narrow beam of light with a wavelength of 0.63 microns from a helium-neon laser was expanded and collimated to a diameter of 5 to 8 cm using a system of confocal lenses, after that it was directed to a film depicting a fractal object whose overall dimensions did not exceed the diameter of the collimated light beam. The picture of the diffraction pattern was formed by a lens in the diffraction plane where the screen was located. Instead of a screen, one can use a digital camera paired with a computer and subject the observed diffraction patterns to the necessary processing.

The computer-generated black-and-white bitmap pictures of the prefractals were approximated by a grid function on a uniform square grid with a number of nodes $n_1 \times n_2$, where the values n_1 and n_2 were chosen sufficiently large (up to 8192) to adequately approximate the details of the smallest size of the prefractal (in computer representation) and to enable the study of prefractals with high generation numbers. For the image digitized in this way, using the fast Fourier transform, the values of the square of the modules of the Fourier components were determined, that is, the spectral distribution of the intensity of diffracted radiation I in the Fraunhofer zone. To display the intensity of diffraction maxima on the plane, circles with a radius proportional to the intensity (or logarithm of intensity) were used, where the proportionality coefficient was chosen for reasons of obtaining optimal clarity of images; for the same purposes, Gaussian blurring of circles was additionally used. The degree of correspondence between the calculated Fourier images and the experimentally observed diffraction patterns depends on the value of the parameter p, equal to the ratio of the smallest element of the fractal to the mesh cell size. The larger the p, the better the match. In our calculations, the value of p was from 4 to 8.

3. METHODS OF CONSTRUCTING BIFRACTALS AND DESCRIPTION OF EXPERIMENTAL RESULTS

As it was indicated in the introduction, that three geometric monofractals were used for the construction of bifractals: a fractal (snowflake) of a Vicsek [2] and two monofractals of the L-system with an axiom ("seed") in the form of a square [4,5] (hereinafter referred to as the LS1 and LS2 fractals). The first fractal has a scaling factor $m = 3$, and theoretical value of dimension $D_f = ln5/ln3 = 1.465$ the last two have $m = 2$ and $D_f = ln3/ln2 = 1.585$. For each of the listed monofractals, megapixel black-and-white bitmap images were created, according to which Fourier images were located.

Fig. 1*a* shows an image of the 3rd generation of the Vicsek prefractal, and Fig. 1*b* (close-up, fractal part) and Fig. 1*c* (general view) – digital diffractograms of this 5th generation prefractal for $p = 8$. Experimental diffractogram for the 5th generation prefractal, presented at two different scales in Fig. 1*d* (close-up, fractal part) and Fig. 1*e* (general view), agree well with the calculated for $p = 8$.

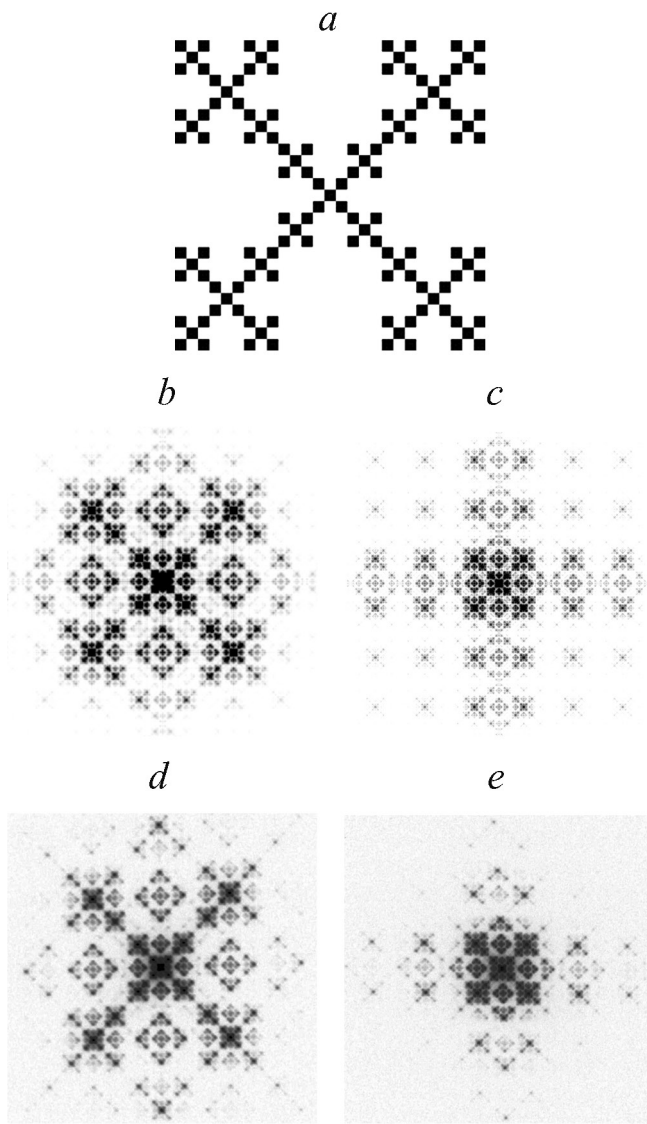

Fig. 1. *Image of the 3rd generation Vicsek prefractal (a), digital diffractograms for the same type prefractal of the 5th generation with p = 8 (b – close-up, c – general view) and experimental diffractograms (d – close-up, e – general view).*

Algorithms for constructing two monofractals LS1 and LS2 with an axiom in the form of a quadrate can be described on the basis of a standard approach for L-systems using a set of rules "turtle graphics", however, in our case, the representation is simpler using the recurrence relations given below, displaying sequential transformations of a single seed a square on the complex plane. Note that this uses transformations using only integer translations of objects along the real and (or) imaginary axes, as well as rotations only by multiples of angles $\pi/2$.

If we choose the orientation of the coordinate system on the complex plane in such a way that the imaginary axis is directed horizontally to the right, and the real axis is directed vertical down, and place the unit seed square (set $Z^{(0)}$) in the first quadrant (coordinates of vertices (0,0), (0,i) (1,i) and (1,0)), then LS1 prefractals of any order (generation) $Z^{(n)}$ are obtained by the operation of combining sets using recurrent relations

$$Z^{(n+1)} = Z^{(n)} \cup \left(iZ^{(n)} + (1+i)2^n\right) \cup \left(-iZ^{(n)} + (1+i)2^n\right) \quad (1)$$

As an example in **Fig. 2**a shows an image of the LS1 fractal of the 4th order resulting from the application of the described procedure, corresponding to the 5th iteration according to formula (1). The calculated for $p = 8$ Fourier

images for a similar fractal of the 10th order are shown in Fig. 2*b* (fractal part, close-up) and Fig. 2*c* (general plan), and experimentally obtained - in Fig. 2*d* (fractal part, close-up) and Fig. 2e (general plan). Digital diffractograms for the LS1 fractal correspond well to experimental ones.

For the LS2 fractal , the chain of successive transformations of the set in the form of a single seed square is given by the expressions

$$Z^{(n+1)} = Z^{(n)} \cup \left(-Z^{(n)} + (2+i)2^n\right) \cup \left(-Z^{(n)} + (1+2i)2^n\right). \quad (2)$$

For example at $n = 5$, we obtain a prefractal of the 4th order, shown in **Fig. 3***a*; diffractograms of the same type of fractal of the 10th order (11th iteration in (2)) for $p = 8$ are shown in Fig. 3*b* (fractal part, close-up) and Fig. 3*c* (general plan). They correspond well to the experimentally obtained Fourier images shown in Fig. 3*d* (fractal part, close-up) and Fig. 3*e* (general plan).

The diffraction patterns, both calculated and experimentally obtained, show that the

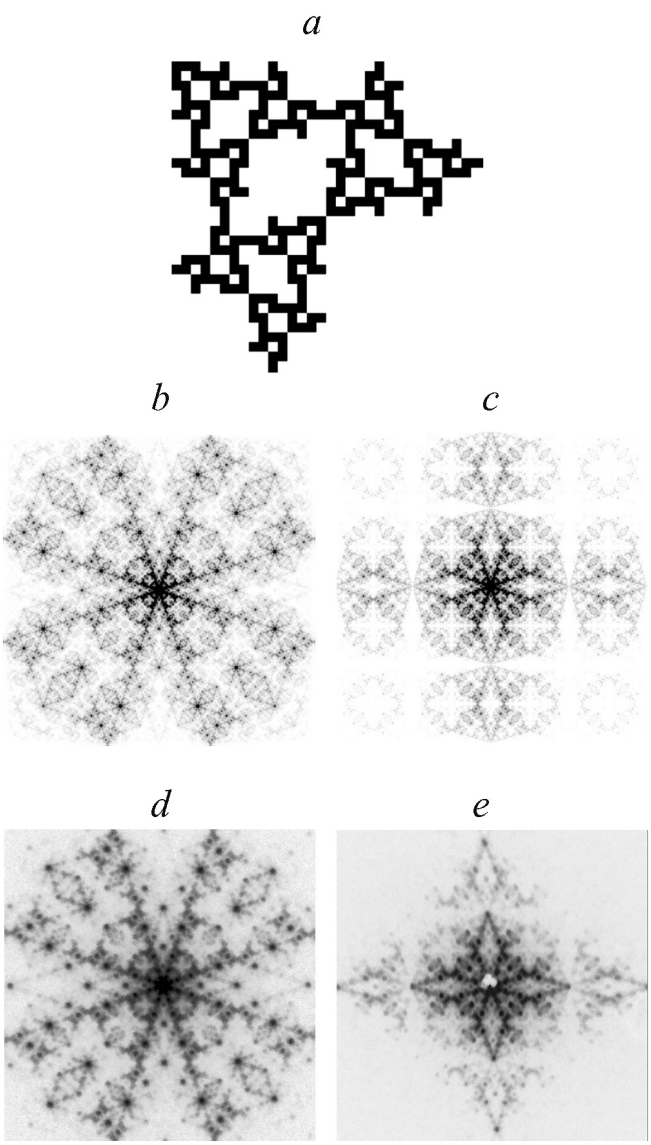

Fig. 2. *Image of the LS1 prefractal of the 4th generation (a), digital diffractograms for the same type of fractal of the 10th generation with p = 8 (b – close-up, c – general view) and experimentally obtained diffractograms (d – close-up, e – general view).*

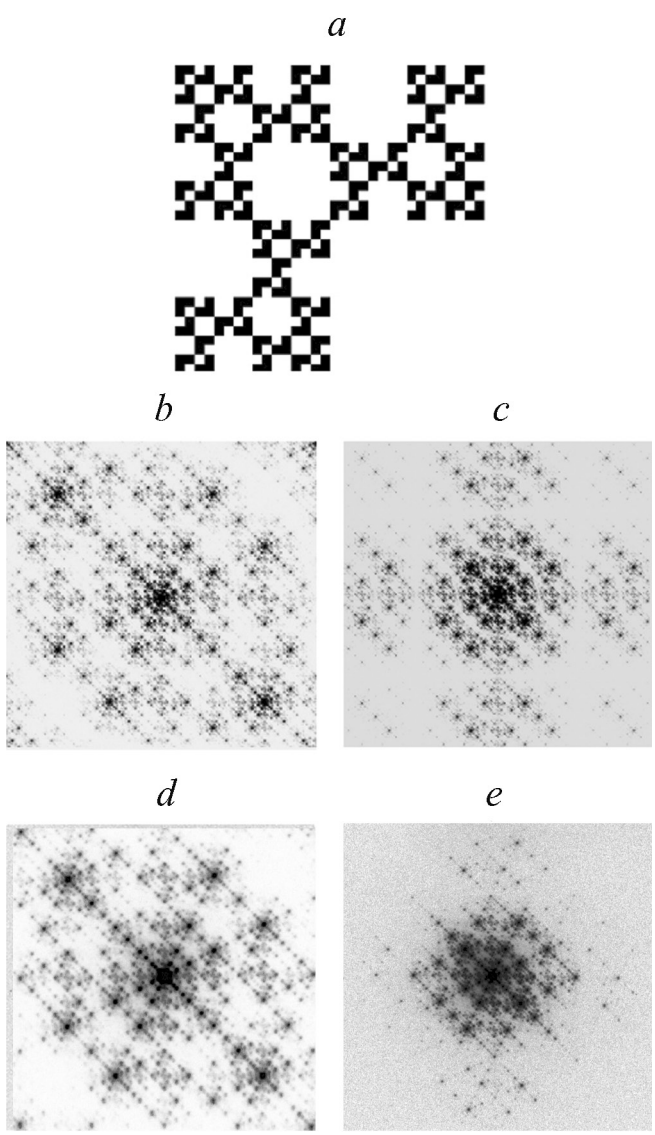

Fig. 3. *Image of the LS2 prefractal of the 4th generation (a), digital diffractograms for the same type of fractal of the 10th generation with p = 8 (b – close-up, c – general view) and experimentally obtained diffractograms (d – close-up, e – general view).*

fractal part has self-similarity with the scaling factor $m = 3$ for the Vicsek fractal (Fig. 1*b*, Fig. 1*d*) and $m = 2$ for LS1 fractals (Fig. 2*b*, Fig. 2*d*) and LS2 (Fig. 3*b*, Fig. 3*d*).

The bibifractals LS1 and LS2 would be formed from two simple geometric monofractals, in one of which (the carrier fractal) the other fractal (the carryable fractal) stood as a seed object. The order of the bifractal obtained in this case is characterized by two indices $k_1 \times k_2$, where k_1 is the order of the carrier fractal, and k_2 is the order of the carryable prefractal. This procedure is fundamentally different from the long-used procedure for creating bifractals (both geometric and "signal") by simply combining two sets.

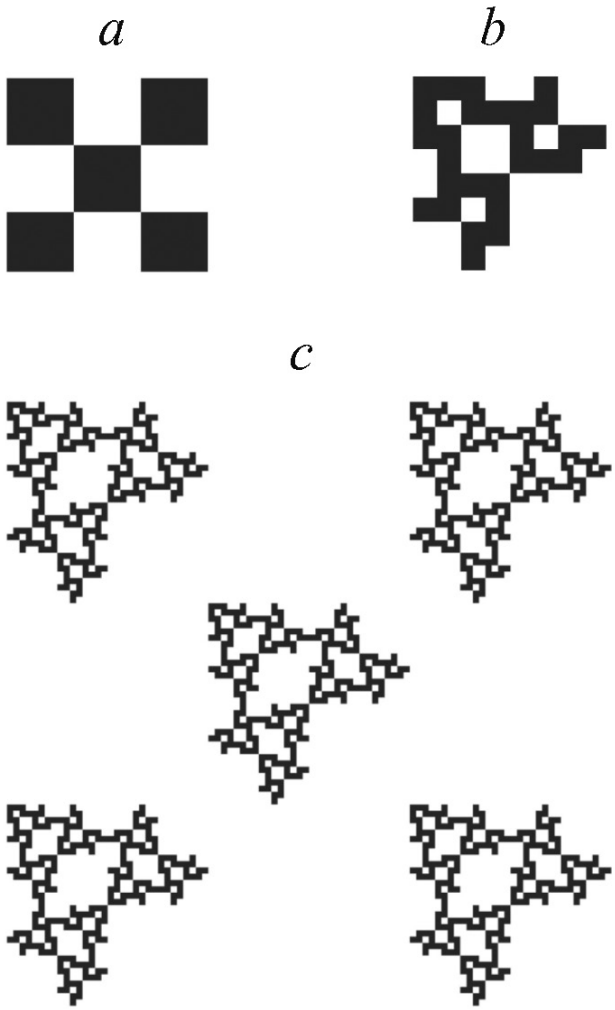

Fig. 4. *The procedure for constructing bifractal No. 1; a – the first generation of Vicsek fractal, b – the second generation of LS1 fractal, c – bifractal No. 1 of 1×4 order.*

The procedure for constructing bifractal No. 1 is shown in **Fig. 4**; the first orders of the Vicsek and LS1 fractals are shown in Fig. 4*a* and Fig. 4*b*, respectively. If the black squares in Fig. 4*a* is replaced by a prefractal LS1 of the 4th order, then you get a bifractal No. 1 of the 1×4 row, the image of which is shown in Fig. 4*c*. In **Fig. 5** shows the diffractograms calculated for different scales for : general plan (Fig. 5*a*), medium (Fig. 5*b*) and large (Fig. 5*c*). Experimental diffractograms are shown in Fig. 5*d* (general plan), Fig. 5*e* (medium plan) and Fig. 5*f* (close-up); they correspond well to the numerical one.

It can be seen that the fine plan of the Fourier image of this bifractal (when considering the "afar"), medium plan on the calculated (Fig. 5*a* and Fig. 5*b*) and experimentally obtained (Fig. 5*d* and Fig. 5*e*) diffractograms generally corresponds to the Fourier image of the LS1 fractal (see Fig. 2*b*-Fig. 2*e*) with scaling factor $m = 2$. But at the same time on the diffractograms of the medium plan (Fig. 5*b* and Fig. 5*e*) the elements characteristic of the diffraction pattern for the Vicsek fractal are already visible (see Fig. 1*b* and Fig. 1*d*). With a further increase in the center of the diffraction pattern (close-up, Fig. 5*c* and Fig. 5*f*) it becomes similar to the Fourier image of the Vicsek

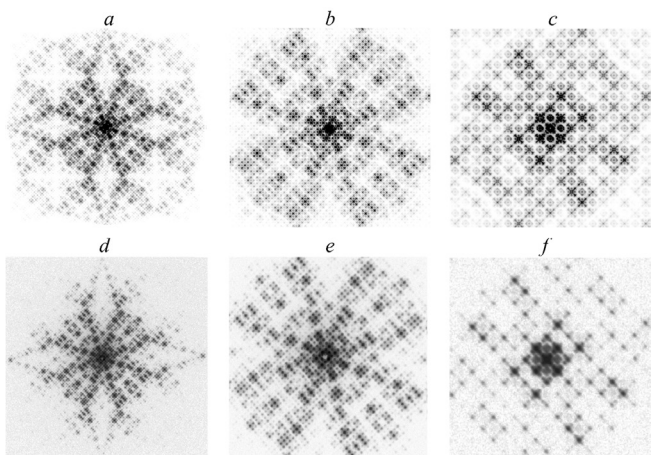

Fig. 5. *Digital diffractograms for bifractal No. 1 for p = 4 (a – general plan, b – medium, c – large) and experimental diffractograms (d – general plan, e – medium, f – large).*

fractal (see Fig. 1*b* and Fig. 1*d*) with a scaling factor $m = 3$. At an intermediate scale (between the scales in Fig. 5*b* (Fig. 5e) and Fig. 5*c* (Fig. 5*f*) self-similarity on diffractograms, calculated and experimental, is lost.

In addition, the entire background of the diffraction pattern is "modulated" in accordance with the pattern for the Vicsek fractal. This phenomenon becomes noticeable at a sufficiently large magnification for any (not only the central) part of the diffraction pattern. Thus, the periphery and rough features of the Fourier image of bifractal No. 1 are called the LS1 fractal, and the central part and "subtle" features are called the Vicsek fractal. With the bifractal itself, the situation is reversed: when viewed "from afar" (small plan), the observer will see the Vicsek fractal, and close up – the LS1 fractal. Thus, both the bifractal itself and its Fourier image are scale-dependent. These features of objects of the "fractal-carrier – carryable fractal" type are typical and were observed in all the bifractals considered in this paper.

The properties of bifractals with the same values of fractal dimension D and scaling coefficients m for the carrier and the carryable object were also studied. In particular, this was done for bifractal No. 2, using as such objects the fractals LS2 and LS1 having the same values $D = 1.585$ and $m = 2$. In **Fig. 6***a* and Fig. 6*b* shows the second generations used in the construction of fractals, in Fig. 6*c* is the resulting bifractal with size 1×4. **Fig. 7** shows the calculated for $p = 4$ diffractograms at different scales: general plan (Fig. 7*a*), medium (Fig. 7*b*) and large (Fig. 7*c*). The experimentally obtained diffractograms are shown in Fig. 7*d* (general plan), Fig. 7*e* (medium plan) and Fig. 7*f* (close-up), which agree well with the calculated ones. Diffractograms in general and medium-scale scales, both calculated and

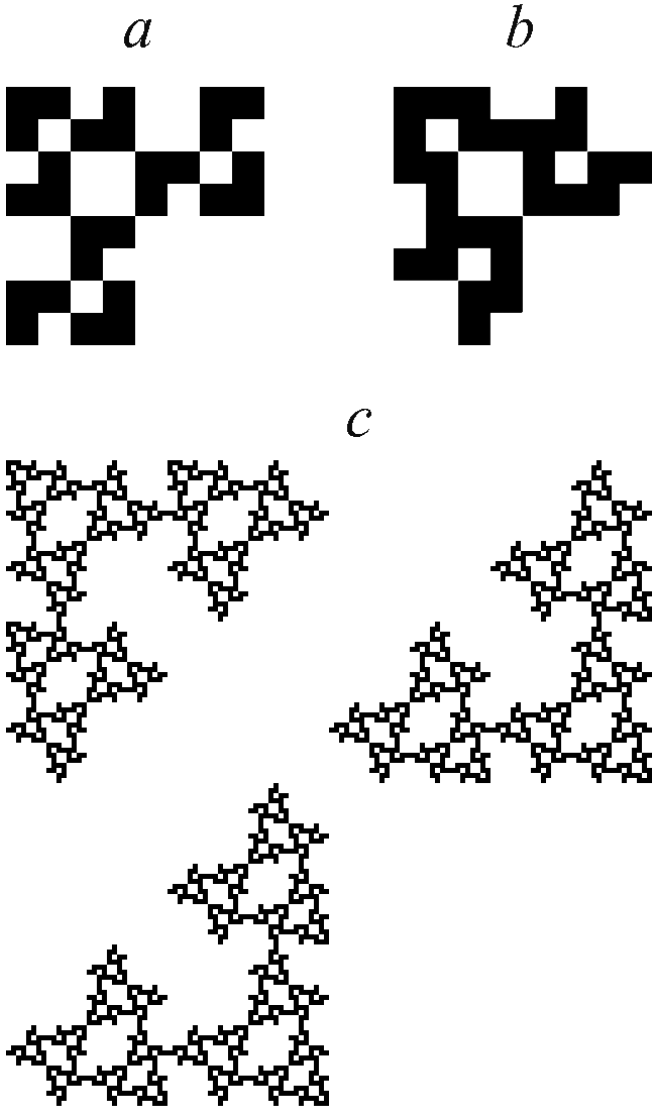

Fig. 6. *The procedure for constructing bifractal No. 2; a and b are the second orders of fractals LS2 and LS1, respectively, c is bifractal No. 2 of 1×4 order.*

experimentally obtained, correspond well to those for the LS1 fractal (Fig. 2*b* - Fig. 2*e*) and have self-similarity with a scaling factor $m = 2$. The central part of the diffractograms (close-up, Fig. 7*c* and Fig. 7*f*) is similar to the Fourier image of the LS2 fractal (Fig. 3*b* and Fig. 3*d*) and also has self-similarity with a scaling factor $m = 2$. Although both the wearable fractal and the carrier fractal have the same scaling coefficient, at some scale intermediate between the scales for medium and small plans, the diffraction pattern loses its self-similarity due to a change in the algorithm for constructing the bifractal.

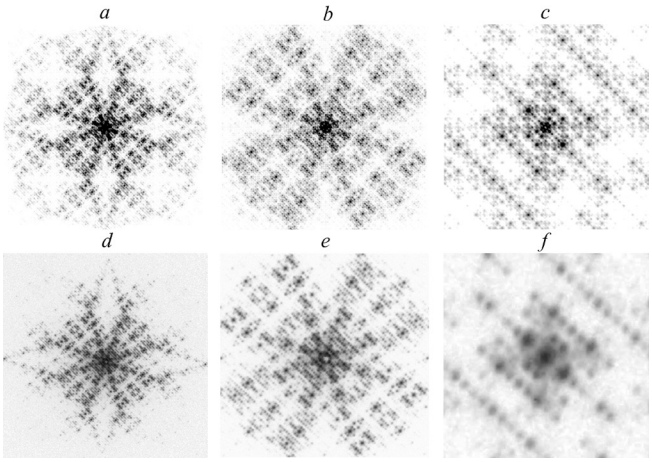

Fig. 7. *Digital diffractograms for bifractal No. 2 for p = 4 (a – general plan, b – medium, c – large) and experimental diffractograms (d – general plan, e – medium, f – large).*

For all the studied geometric fractals, the difference between the central and peripheral parts is observed on the digital diffractograms and diffraction patterns experimentally obtained by the optical method. The part localized near the center has the self-similarity inherent in fractal objects (see Fig. 1*b* and Fig. 1*d*, Fig. 2*b* and Fig. 2*d*, Fig. 3*b* and Fig. 3*d*), while the peripheral part, which does not possess self-similarity, is characterized by an equidistant arrangement of diffraction maxima along a certain number of radial directions (rays) (see, for example, Fig. 1*c* and Fig. 1*e*). For the first time, this fact was noticed by the authors of the work [14] devoted to the study of Fraunhofer optical diffraction on the classical Koch snowflake, where they used the terms "fractal part" and "lattice part" to denote the central and peripheral parts and associated the appearance of the latter with the fact that in a two-dimensional set of elements forming a fractal, one-dimensional diffraction gratings consisting of identically oriented elements (e.g. segments) can be distinguished.

For bifractals, this effect also takes place. The rough pattern of the lattice part of the bifractal diffractogram is determined by the carryable fractal, but, in addition, it (like the entire diffraction pattern) is modulated by a carrier fractal. The rough drawing of the periphery of the fractal part is also determined by the carryrable fractal, and only the very center of the diffraction pattern corresponds to the diffractogram of the carrier fractal; the size of this part depends on the number of orders in the carrier fractal and the ratio of orders in both fractals.

4. CONCLUSION

A careful comparison of the diffraction patterns observed in experiments for bifractals based on the classical Vicsek fractal and two fractals of the L-system with Fourier images of bifractals approximated by a grid function on a uniform square grid allowed us to formulate certain requirements for the approximation process. It has been shown that almost complete correspondence of experimental and digital diffractograms and good reproduction of the fine structure of the former is achieved with a sufficiently high ratio of the size of the smallest element of the bifractal to the period of the grid function.

All the obtained Fourier images of bifractals, both calculated and experimentally observed, were scale-dependent. The diffractograms of the small plan ("far") of the lattice and fractal parts corresponded to the wearable fractal, the close-up ("near") – to the carrierable fractal. At some intermediate scale, self-similarity was violated. All parts of the diffraction pattern, both central and peripheral, had a fine structure modulated in accordance with the Fourier image of the wearable fractal, which could be seen with sufficient magnification.

REFERENCES

1. Arzamastseva GV, Evtikhov MG, Lisovsky FV, Mansvetova EG. Svoystva ploskih geometric bifractals. *RENSIT: Radioelectronics. Nanosystems. Information Technologies*, 2012, 4(2):93-107 (in Russ.).
2. Vicsek T. Fractal model for diffusion controlled aggregation. *J. Phys. A*, 1983, 16(17):1647-1652.
3. Loskutov AYu, Mihaylov AS. *Osnovy teorii slozhnykh sistem*. Moscow-Izhevsk, Institut comp`yuternyh issledovaniy Publ., 2007, 620 s (in Russ.).
4. Lindermayer A. Mathematical model for cellular interaction in development. I. Filaments with one-sided inputs. *J. Theor. Biol.*, 1968, !8(3):280-299.
5. Lindermayer A. Mathematical model for cellular interaction in development. II. Simple and branching filaments with two-sided inputs. *J. Theor. Biol.,* 1968, !8(3):300-315.
6. Arzamastseva GV, Evtikhov MG, Lisovsky FV, Lukashenko LI. Comp`yuternoe modelirovanie difraktsii na fractal'nyh domennyh structurah. *Tr. XIX Merzdunarod. Shkoly-seminara "Novye magnitnye materialy microelectroniki"*, Moscow, 2004, c. 632-634 (in Russ.).
7. Lisovsky FV, Lukashenko LI, Mansvetova EG. Termodinamicheski ustoychivye fractalopodobnye domennye struktury v magnitnykh plenkakh. *Pis`ma v ZHETF*, 2004, 79(7):432-435 (in Russ.).
8. Arzamastseva GV, Evtikhov MG, Lisovsky FV, Mansvetova EG, Temiryazeva MP. Amorfizatsiya biperiodicheskikh domennykh struktur v kvaziodnoosnykh magnitnykh plenkakh kriticheskoy tolshchiny. *ZHETF*, 2008, 134(2):282-290 (in Russ.).
9. Arzamastseva GV, Evtikhov MG, Lisovsky FV, Mansvetova EG. Fur'e obrazy fraktal'nyh ob'ektov. *Izv. RAN, Ser. fiz.*, 2010, 74(10):1430-1432 (in Russ.).
10. Arzamastseva GV, Evtikhov MG, Lisovsky FV, Mansvetova EG. Comp'yuternoe modelirovanie difraktsii Fraungofera na H-fraktalakh i krivykh Peano. *Electromagnitnye volny i electronnye sistemy*, 2012, 17(7):48-58 (in Russ.).
11. Arzamastseva GV, Evtikhov MG, Lisovsky FV, Mansvetova EG. Family of Generalized Triadic Koch Fractals: Dimensions and Foirier Images. *RENSIT: Radioelectronics. Nanosystems. Information nechnologies*, 2016, 8(1):81-90. DOI: 10.17725/rensit.2016.08.081.
12. Arzamastseva GV, Evtikhov MG, Lisovsky FV, Mansvetova EG. Foirier Images Quasisymmetry of Generalized Triadic Koch Prefractals. *RENSIT: Radioelectronics. Nanosystems. Information nechnologies*, 2016, 8(2):207-214 DOI: 10.17725/rensit.2016.08.207.
13. Arzamastseva GV, Evtikhov MG, Lisovsky FV, Mansvetova EG. Light Diffraction by Fractals: Comparison of Experimental Data With the Obtained by Numerical Methods Fourier Images of the Object Pictures. *RENSIT: Radioelectronics. Nanosystems. Information nechnologies*, 2017, 9(2):221-229. DOI: 10.17725/rensit.2017.09.221.
14. Uozumi J, Kimura H, Asakura T. Fraunfofer diffraction by Koch Fractals. *J. Mod. Optics Phys.*, 1990 37(6):1011-1031.